Analysis of Shear-Critical Reinforced Concrete Plane Frame Elements under Cyclic Loading

Serhan Guner[1] and Frank J. Vecchio, M.ASCE[2]

Abstract: An analytical procedure was recently developed for the nonlinear analysis of reinforced concrete frame structures consisting of beams, columns, and shear walls under monotonic loading. The procedure is distinct from others because it is capable of inherently and accurately considering shear effects and significant second-order mechanisms with a simple modeling process suitable for use in practice. In this study, the procedure is further developed to enable the performance assessment of shear-critical frame structures under general (arbitrary) loading, including the special cases of cyclic and reversed-cyclic loads. Newly developed and implemented formulations are described and applied to 11 previously tested specimens for verification. Important considerations in nonlinear modeling and the limitations of the procedure are also discussed. The procedure is found to accurately simulate the overall experimental behaviors of the specimens examined. Performance measures, such as load and deformation capacities, stiffnesses, energy dissipations, ductilities, failure modes, crack widths, and reinforcement strains, are typically captured well. The procedure exhibits excellent convergence and numerical stability, requiring little computational time. **DOI: 10.1061/(ASCE)ST.1943-541X.0000346.**

CE Database subject headings: Cyclic loads; Reinforced concrete; Nonlinear analysis; Shear; Beam columns; Earthquake loads; Frames; Hysteresis.

Author keywords: Beam columns; Cyclic loads; Earthquake loads; Fiber models; Frame structures; Hysteresis; Nonlinear analysis; Reinforced concrete; Shear.

Introduction

In the performance assessment of frame structures, it is common to perform a nonlinear static pushover analysis to determine the strength, ductility, sequence of nonlinear occurrences, and failure mode of the frame. With such monotonic loading conditions, failures because of shear effects typically occur in either deep members or in improperly designed members with inadequate shear reinforcement details and amounts. Flexural failures prevail in properly designed slender members typically encountered in the majority of existing frame systems. However, under cyclic loads, such as earthquake excitation, shear-related mechanisms tend to dominate the behavior of even flexure-critical elements. It may be stated that ultimately all failures under cyclic loads are shear failures incurred by either desegregation of concrete between doubly diagonal cracks or the localized slip between two faces of large flexural cracks (Petrangeli et al. 1999). Therefore, consideration of shear-related mechanisms is essential for accurate simulations of frame behavior under cyclic loads.

In the nonlinear analysis of frame structures, one-dimensional (1D) distributed (spread) nonlinearity fiber beam models employing various constitutive relationships represent the most common approach because of their computational efficiency and analytical accuracy. Although several procedures have been proposed involving reinforced concrete fiber beam elements under monotonic loads, only a small number of them consider shear effects. Among them are the formulations by Bazant and Bhat (1977), Vecchio and Collins (1988), Rericha (1991), Bentz (2000), Filippou and Saritas (2006), Mostafaei and Vecchio (2008), and Guner and Vecchio (2010a). However, frame analysis methods available for cyclic loading, which consider shear-related effects, are fewer still. The ones that do exist tend to be either overly complex with limited practicality or overly simplified with limited validity.

One viable procedure, proposed by Petrangeli et al. (1999), involves a force-based fiber beam element with a concrete constitutive model based on the microplane theory. The procedure includes two options for the sectional shear strain distribution assumed and two options for the equilibrium in the transverse direction. Although it is an advanced and well-developed model, its complex formulations present difficulties in their implementation into standard finite-element procedures and demand considerable computational effort. In addition, the model requires the input of several parameter values, such as the total fracture energy per unit length and estimated crack spacing, which further limits its use to specialists with advanced modeling experience. Marini and Spacone (2006) significantly simplified Petrangeli's method and proposed a force-based fiber beam element by using a phenomenological shear stress-strain law based on Eurocode 2 [European Committee for Standardization (CEN) 1991]. Although computationally fast and efficient, the model possesses deficiencies regarding shear modeling; one such compromise is the uncoupled treatment of bending and axial responses from the shear response at the sectional level. The model also neglects important second-order mechanisms, such as aggregate interlock, reinforcement dowel action, and concrete out-of-plane confinement effects.

Bairan and Mari (2007) proposed a three-dimensional (3D) beam model that uses a smeared-crack approach to consider the

[1]Structural Engineer, Morrison Hershfield Ltd., Suite 600, 235 Yorkland Blvd., Toronto ON, Canada M2J 1T1 (corresponding author). E-mail: s.guner@utoronto.ca

[2]Professor, Dept. of Civil Engineering, Univ. of Toronto, 35 St. George St., Toronto ON, Canada M5S 1A4.

Note. This manuscript was submitted on December 18, 2008; approved on October 6, 2010; published online on December 16, 2010. Discussion period open until January 1, 2012; separate discussions must be submitted for individual papers. This paper is part of the ***Journal of Structural Engineering***, Vol. 137, No. 8, August 1, 2011. ©ASCE, ISSN 0733-9445/2011/8-834–843/$25.00.

coupled actions of bending, shear, torsion, and axial forces. This model requires that the cross sections be discretized into a finite-element mesh using two-dimensional (2D) concrete and 1D steel elements. Consequently, it requires considerable modeling effort and analysis time, which limits its application to special investigations. Ceresa et al. (2009) proposed a displacement-based fiber beam element, using a smeared-crack approach and a uniform shear strain distribution assumption. This method requires the input of only basic material properties; therefore, it is suitable for practical applications. However, there are a number of areas requiring further development, as reported by its authors. Among them are the numerical difficulties encountered during the analyses and the deficiencies in capturing the degradation of the postpeak strength and stiffness under cyclic loads.

There remains a significant need for the development of practical and accurate analysis tools that can be used by structural engineers for common applications. The available methods, as discussed previously, are highly useful to researchers for special investigations. However, they typically require extensive knowledge of nonlinear modeling and material behavior and the selection of appropriate analysis options and parameter values. The practical methods, on the other hand, tend to have deficiencies in their shear modeling and general applicability. Thus, the objective of this study is to compliment the literature with a practical analytical procedure that inherently and accurately considers shear effects. It also seeks to considerably reduce or eliminate the need for preanalysis calculations, such as development of sectional response hystereses and strength interaction relationships, and simplify the selection or determination of parameter values and analysis options.

In this current study, formulations previously proposed for monotonic loading are further developed to enable an analysis capability under general (arbitrary) loading. The main framework of the analytical procedure is described by Guner and Vecchio (2010a). Here, only the newly implemented formulations added to the existing procedure are presented. Furthermore, a verification study is presented through the application of the procedure to a variety of previously tested specimens. Important considerations in nonlinear modeling, such as the selection of member lengths and creation of sectional models, and the limitations of the procedure are also discussed.

Overview of Analysis Methodology

Based on a total load, iterative, secant-stiffness formulation, the computer-based calculation procedure consists of two interrelated analyses. First, a linear-elastic global frame analysis using a classical stiffness–based Euler-Bernoulli beam element with six degrees of freedom is performed to obtain member end actions and deformations. Using the calculated deformations, nonlinear sectional analyses are performed to determine the member sectional forces based on a distributed-nonlinearity fiber approach. The differences between the global and sectional forces are termed the *unbalanced forces*, which are added to the *compatibility restoring forces* (i.e., virtual static loads) to force member deformations in the global frame analysis to match those in the nonlinear sectional analyses. The compatibility restoring forces are applied to the ends of each member in a self-equilibrating manner. The global frame analysis and the sectional analyses are performed iteratively until all unbalanced forces converge to zero.

A layered (fiber) analysis technique is employed for the sectional analyses, in which the cross section is divided into a number of concrete, longitudinal reinforcing bar and longitudinal prestressing steel layers, as shown in Fig. 1. Transverse reinforcement is

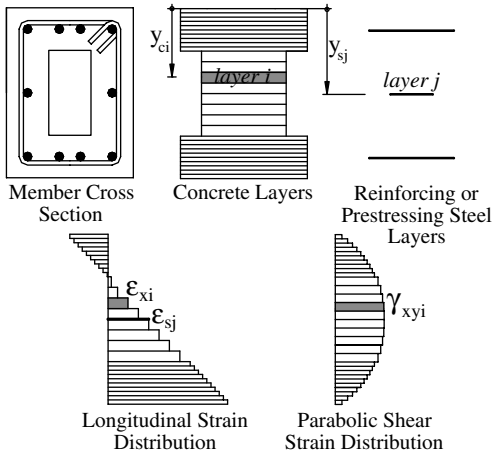

Fig. 1. Layered section analysis technique proposed

smeared within the concrete layers. Each layer is then analyzed for 2D in-plane strain conditions according to the equilibrium, compatibility, and constitutive requirements of the disturbed stress field model (DSFM) (Vecchio 2000). The main sectional compatibility requirement enforced is that "plane sections remain plane," and the sectional equilibrium requirements include balancing the axial force, shear force, and bending moment calculated by the global frame analysis. While the clamping stresses in the transverse direction are assumed to be zero, a shear protection algorithm is employed to prevent premature failures of D-regions. As is typical with sectional analysis methods using the beam theory, the proposed method is only suitable for the analysis of B-regions (i.e., slender members with shear span-to-depth ratios greater than 2.0). The method should not be used for the local analysis of D-regions.

For the consideration of shear, a parabolic shear strain distribution through the section depth is assumed. Verification studies performed by Vecchio and Collins (1988), Petrangeli et al. (1999), and Guner and Vecchio (2010b) demonstrated that the parabolic strain assumption provides good correlations to the experimental section behaviors. Furthermore, it enables fast and robust analysis and a capability to continue an analysis into the postpeak region to determine frame ductility, which is perhaps the most sought performance measure, next to strength, in a frame analysis. Detailed discussion of the use of a predefined shear strain distribution is provided by Vecchio and Collins (1988).

At the conclusion of an analysis, the procedure, which is implemented in the computer code VecTor5 (Guner and Vecchio 2008), provides sufficient output to fully describe the behavior of the structure, including the load-deflection response, member deformations, concrete crack widths, reinforcement stresses and strains, deficient members if any, failure mode, and failure displacement of the structure. The postpeak response of the structure is also provided, from which the energy dissipation and the displacement ductility can be calculated. The procedure allows for the analysis of frames with unusual or complex cross sections under a wide range of static and thermal load conditions. A more detailed description of the procedure is provided by Guner and Vecchio (2010a).

Modifications for General Loading Conditions

A method of analysis was developed by Vecchio (1999) for 2D continuum elements by which a secant-stiffness-based finite-element algorithm, employing a smeared rotating crack assumption,

can be modified to incorporate an analysis capability under general loading. The same study also proposed a constitutive model for concrete that included simple unloading and reloading rules based on a plastic offset formulation. In a later study, Palermo and Vecchio (2003) developed a more comprehensive constitutive model for concrete, which additionally included a degradation in strength in the reloading curves, calculation of plastic offsets in both the tension and compression domains, and consideration of partial unloading and reloading in both the tension and compression domains.

In this study, the method of analysis developed by Vecchio (1999) is implemented into the proposed procedure as the main framework for general load analysis. Furthermore, three constitutive models for concrete, including the Palermo and Vecchio (2003) model, and three constitutive models for reinforcement are incorporated. The majority of the implementations are made in the sectional analysis algorithm, in which the stress and strain calculations are carried out for each concrete and steel layer. Additionally, the global frame analysis subroutine is modified to update the concrete and steel stress and strain histories at the end of each load stage. Details of the modifications are provided in the following sections.

Consideration of Plastic Offset Strains

In the monotonic loading formulation of the proposed procedure, as presented by Guner and Vecchio (2010a), total concrete strains were formulated to include concrete plastic offset strains caused by cyclic loading and damage. Similarly, total reinforcement strains contained plastic offset strains caused by cyclic loading and yielding. Both plastic offset components, however, were taken as zero because the method was only able to consider monotonic loading. In this current study, to enable an analysis capability under general loading, a plastic offset formulation is implemented to consider the concrete and reinforcement plastic strains as a part of the total strains.

In this implementation, the plastic offset strains incurred by the concrete under load reversals must be defined and retained. Because a rotating crack approach is used, the principal strain directions are free to rotate; therefore, the plastic offset strains must be defined with respect to the local x- and y-axes so that the previous damage does not rotate with the rotation of the principal strain directions. For this purpose, an incremental formulation is employed, patterned after Vecchio (1999), at each sectional analysis iteration performed for each concrete layer. In this calculation, previously stored concrete plastic offset strains ε^p_{cx}, ε^p_{cy}, γ^p_{cxy} are transformed into principal concrete plastic offset strains ε^p_{c1}, ε^p_{c2}. This transformation is performed through the standard transformation equations (see Vecchio 1999), in which the elastic strain components, not the total strains, are used to determine the current orientation of the stress field θ. At the same time, the instantaneous concrete plastic offset strains are calculated on the basis of the selected concrete hysteresis model. The Palermo and Vecchio (2003) model, for example, formulates the concrete plastic offset strains in the compression and tension domains, as defined by Eq. (1) and Eq. (2), respectively:

$$\varepsilon_c^{p,\text{ins}} = \varepsilon_p \times [0.166 \times (\varepsilon_{cc}/\varepsilon_p)^2 + 0.132 \times (\varepsilon_{cc}/\varepsilon_p)] \quad (1)$$

$$\varepsilon_c^{p,\text{ins}} = 146 \times \varepsilon_{ct}^2 + 0.523 \times \varepsilon_{ct} \quad (2)$$

where ε_{cc} and ε_{ct} = unloading strains from the compression and tension backbone curves; and ε_p = strain corresponding to the peak stress in the base curve [Vecchio 2000, Fig. 9(a)]. The typical hysteretic response obtained from this model is shown in Fig. 2.

If the instantaneous plastic offset strains exceed the previously stored plastic offset strains, ε^p_{c1} and ε^p_{c2}, incremental plastic offset strains are generated, which can be compressive or tensile in either of the principal directions as follows:

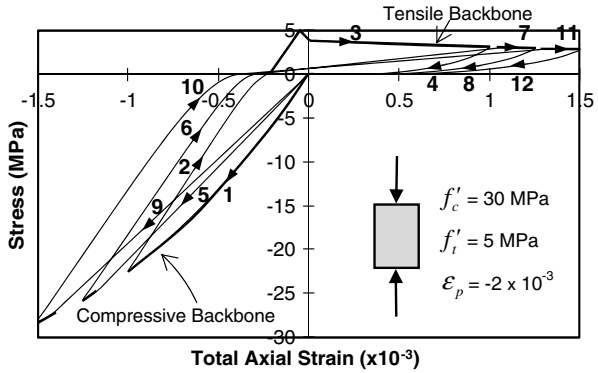

Fig. 2. Palermo and Vecchio model: concrete response under reversed-cyclic strain excursions

$$\Delta\varepsilon^p_{c1} = \varepsilon_c^{p,\text{ins}} - \varepsilon^p_{c1} \quad (3)$$

$$\Delta\varepsilon^p_{c2} = \varepsilon_c^{p,\text{ins}} - \varepsilon^p_{c2} \quad (4)$$

At the end of each load stage of the global frame analysis, previously stored concrete plastic offset strains are updated for all concrete layers as follows:

$$\varepsilon_{cx}^{p,\text{new}} = \varepsilon^p_{cx} + \Delta\varepsilon^p_{c1} \times (1 + \cos 2\theta)/2 + \Delta\varepsilon^p_{c2} \times (1 - \cos 2\theta)/2 \quad (5)$$

$$\varepsilon_{cy}^{p,\text{new}} = \varepsilon^p_{cy} + \Delta\varepsilon^p_{c1} \times (1 - \cos 2\theta)/2 + \Delta\varepsilon^p_{c2} \times (1 + \cos 2\theta)/2 \quad (6)$$

$$\gamma_{cxy}^{p,\text{new}} = \gamma^p_{cxy} + \Delta\varepsilon^p_{c1} \times \sin 2\theta - \Delta\varepsilon^p_{c2} \times \sin 2\theta \quad (7)$$

The plastic offset strains incurred in each longitudinal steel layer and smeared transverse reinforcement component are treated similarly. Because of their fixed orientations, the calculation is significantly simplified, requiring only two equations similar to Eqs. (3) and (4).

Consideration of Maximum and Minimum Strains

Concrete hysteresis models typically require the knowledge of previously attained maximum and minimum concrete strains. This is because in most models (including those implemented), concrete stresses are calculated from a set of rules linked to the backbone curve that corresponds to the monotonic response of the concrete.

Analogous to the plastic offset formulation, because cracks are free to rotate, an incremental formulation is adopted after Vecchio (1999) for the calculation of maximum and minimum concrete strains attained. Consider first the maximum compressive strains in the concrete. At each sectional analysis iteration performed for each concrete layer, previously stored maximum total concrete strains ε_{cmx}, ε_{cmy}, γ_{cmxy} are transformed into principal directions as ε_{cm1} and ε_{cm2} based on the current orientation of the stress field θ. If the current total concrete compressive strains, ε_{c1} and ε_{c2}, exceed the previously stored maximum compressive strains, ε_{cm1} and ε_{cm2}, incremental concrete total strains are generated as follows:

$$\Delta\varepsilon_{cm1} = \varepsilon_{c1} - \varepsilon_{cm1} \quad (8)$$

$$\Delta\varepsilon_{cm2} = \varepsilon_{c2} - \varepsilon_{cm2} \quad (9)$$

At the end of each load stage of the global frame analysis, previously stored maximum concrete compressive strains are updated for all concrete layers as follows:

$$\varepsilon_{cmx}^{\text{new}} = \varepsilon_{cmx} + \Delta\varepsilon_{cm1} \times (1 + \cos 2\theta)/2 + \Delta\varepsilon_{cm2} \times (1 - \cos 2\theta)/2 \quad (10)$$

$$\varepsilon_{cmy}^{\text{new}} = \varepsilon_{cmy} + \Delta\varepsilon_{cm1} \times (1 - \cos 2\theta)/2 + \Delta\varepsilon_{cm2} \times (1 + \cos 2\theta)/2 \quad (11)$$

$$\gamma_{cmxy}^{\text{new}} = \gamma_{cmxy} + \Delta\varepsilon_{cm1} \times \sin 2\theta - \Delta\varepsilon_{cm2} \times \sin 2\theta \quad (12)$$

The maximum tensile strains ε_{tmx}, ε_{tmy}, and γ_{tmxy} are calculated and stored in a similar manner. In addition, previously attained maximum and minimum reinforcement strains are calculated through the use of two simple equations, similar to Eqs. (8) and (9), for each reinforcement component.

Stress-Strain Models for Concrete

Three alternative concrete constitutive models are implemented into the analytical procedure: the Vecchio (1999) model with linear unloading; the Vecchio (1999) model with nonlinear unloading, which is the default model because of its simplicity; and the Palermo and Vecchio (2003) model with cyclic decay. These models are used in the sectional calculations to calculate concrete principal stresses corresponding to the concrete principal strains.

Stress-Strain Models for Reinforcement

Three alternative constitutive models are implemented for the stress calculations of the longitudinal reinforcement: a basic elastic-plastic model, an elastic-plastic model with strain hardening, and the Seckin (1981) model with Bauschinger effects, which is the default model. For the transverse reinforcement, the only formulation implemented is the elastic-plastic with strain hardening. The details of the Seckin model, as implemented, are provided by Vecchio (1999). For illustrative purposes, the response of a reinforcement component to a monotonically increasing strain excursion of $\pm 2.5 \times 10^{-3}$ is given in Fig. 3.

Application to Frames

The frame specimen tested by Duong et al. (2007), a one-bay, two-story shear-critical frame, as shown in Fig. 4, was examined. The experiment consisted of two test phases. In Phase A, the frame was loaded under increasing imposed lateral displacement until significant shear damage developed in the beams before being unloaded completely. The frame was then reloaded in the reverse direction to approximately the same lateral displacement (44 mm) attained in the forward half-cycle and, finally, was unloaded.

This frame was previously analyzed by Guner and Vecchio (2010b) by using the analysis procedure proposed for the monotonic loading phase. Here, the same frame model was used for an analysis under a reversed-cyclic loading in a displacement-controlled mode to simulate Phase A loading. As seen in Fig. 5(a), the shear-critical response of the frame was calculated with a high degree of accuracy. The strength of the frame in both directions was calculated to within approximately 5% of the experimental values. The total energy dissipated by the frame was also calculated with good accuracy, as shown in Table 1, wherein DF+ and DF− denote the positive and negative loading directions, respectively. Upon unloading, the residual displacement was calculated with a reasonable

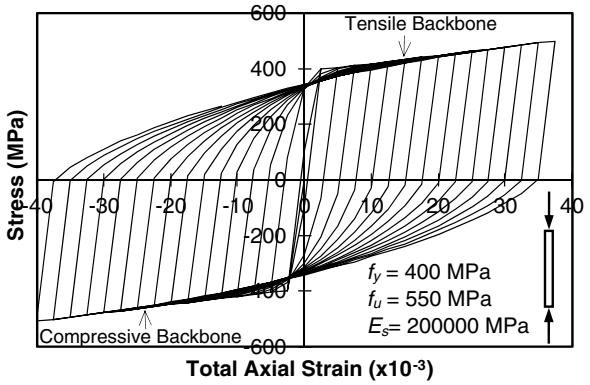

Fig. 3. Seckin model: reinforcement response under reversed-cyclic strain excursions

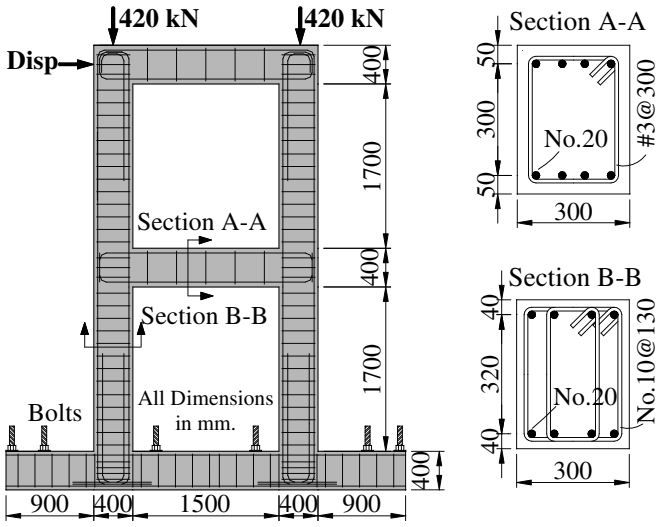

Fig. 4. Structural details of Duong et al. (2007) frame

8% underestimation. The lateral load levels causing the first yielding of several reinforcement components, overall reinforcement strain responses, flexural and shear crack widths, and column and beam axial deformations were estimated reasonably well, as documented by Guner (2008).

The experimentally observed damage mode of the frame in the reverse half-cycle was shear-dominated, with significant damage (7.0 mm maximum crack width) to the central portion of the first-story beam. In the analytical study, shear failures at both ends of the first-story beam (4.0 mm maximum crack width) occurred. In Fig. 5(a), the drop in the load capacity from 311 kN to 165 kN at a lateral displacement of −40 mm occurred because of these failures.

To demonstrate the influence of shear-related mechanisms, the frame analysis was repeated ignoring shear effects. As seen in Fig. 5(b), the overall response of the frame is computed inaccurately. The strength was overestimated by 14%; upon unloading, the residual displacement was overestimated by 65%. The failure mode of the frame was calculated to be flexural with reinforcement fractures and concrete crushing at both ends of both beams. The biggest inaccuracy was in the displacement ductility prediction, which was erroneously calculated as 9.0 times the experimental ductility. This example shows the importance of considering shear effects to avoid erroneous and dangerously unsafe predictions of structural performance.

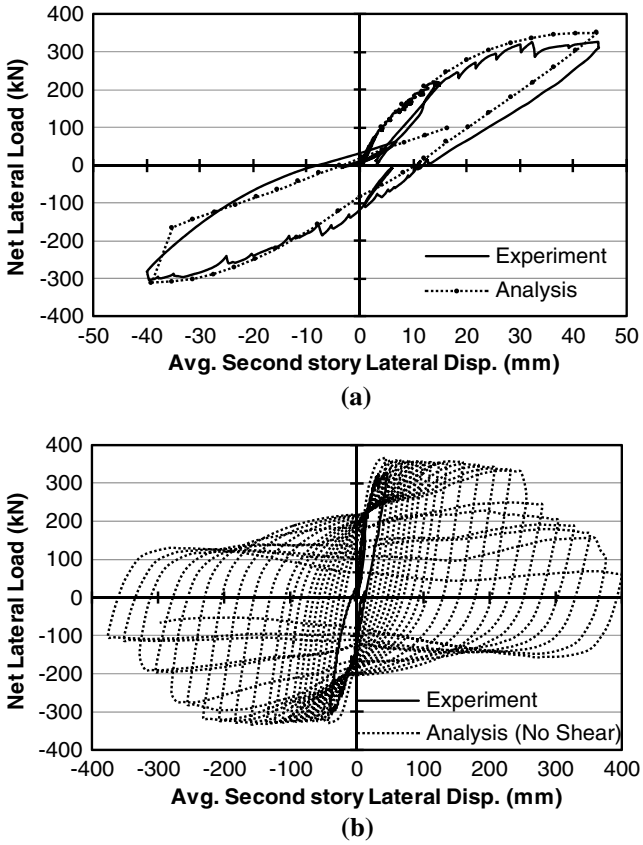

Fig. 5. Comparison of load-deflection responses for Duong et al. (2007) frame: (a) considering shear effects; (b) neglecting shear effects

Application to Beam-Column Subassemblies

The first set of specimens examined was those tested by Seckin (1981), involving a number of exterior beam-column subassemblies. Examined here are Specimens SP6 and SP7, both of which sustained the least joint core damage among all the specimens in this experimental program. The proposed procedure is not currently suitable for modeling joint core distress, as will be discussed in the subsequent limitations section. Both specimens had identical details, with the exception of joint core tie spacing and material properties. Because stiffened joint core members are employed in the model, small differences in the reinforcement amount in these regions will not be significant in the analysis. The concrete compressive strengths used were approximately 37 and 31 MPa for SP6 and SP7; the reinforcement yield strength was about 350 MPa, as reported by Seckin (1981). The test program involved applying a vertical force to the tip of the beam and a constant axial load to the column, as shown in Fig. 6. An arbitrary loading protocol was used for the beam tip loading, as shown in Fig. 7.

The frame analysis procedure employed requires that frame elements be divided into reasonably short members to ensure that the average member forces are reasonably calculated. However, it was found in some cases that the use of excessively small member lengths may cause deteriorated accuracy. This anomaly arises from the calculation of the shear compatibility restoring forces, which are a function of the member sizes used. Consequently, using excessively short members increases the shear compatibility restoring forces and may cause less ductile responses, especially for shear-dominated structures. Neither stiffness nor strength is found to be affected by this considerably. From the results of a parametric study, Guner (2008) recommended using member lengths for frame structures in the range of one-half of the cross-section depths for

Table 1. Comparison of Analytical and Experimental Results

	Peak force (kN)			Corresponding displacement (mm)			Energy dissipation (kN • m)		
	Analysis	Experiment	Ratio	Analysis	Experiment	Ratio	Analysis	Experiment	Ratio
DF+	348	327	1.06	45	45	0.99	11.3	11.0	1.03
DF−	−311	−304	1.03	−39	−40	0.98	9.6	10.0	0.96
SP6+	121	117	1.04	126	189	0.67	119.6	93.8	1.28
SP6−	−75	−83	0.91	−96	−54	1.78	81.7	78.3	1.04
SP7+	122	111	1.10	135	135	1.00	79.7	59.4	1.34
SP7−	−77	−86	0.90	−120	−114	1.05	52.6	39.8	1.32
A2+	74	79	0.93	29	29	1.00	25.3	22.2	1.14
A2−	−74	−76	0.97	−44	−59	0.75	22.4	18.9	1.19
A3+	173	178	0.97	30	29	1.04	52.1	39.9	1.31
A3−	−121	−123	0.99	−44	−59	0.75	40.3	33.4	1.21
B1+	260	282	0.92	100	100	1.00	113.7	102.8	1.11
B1−	−248	−289	0.86	−100	−75	1.33	122.3	110.9	1.10
B2+	664	692	0.96	125	100	1.25	349.6	287.7	1.22
B2−	−631	−709	0.89	−100	−100	1.00	378.5	287.2	1.32
B7+	976	1,004	0.97	125	125	1.00	576.6	501.3	1.15
B7−	−972	−1,011	0.96	−125	−125	1.00	588.9	521.8	1.13
B8+	964	968	1.00	125	100	1.25	677.1	573.8	1.18
B8−	−962	−1,064	0.90	−125	−121	1.03	594.8	594.8	1.03
R1+	115	121	0.95	100	75	1.33	81.6	74.5	1.10
R1−	−111	−120	0.92	−100	−100	1.00	74.0	69.2	1.07
F1+	844	852	0.99	100	100	1.00	202.4	169.3	1.20
F1−	−765	−818	0.93	−100	−77	1.30	228.2	188.4	1.21
		Mean	0.96		Mean	1.07		Mean	1.16
	(%)	COV	5.9		COV	23.7		COV	10.6

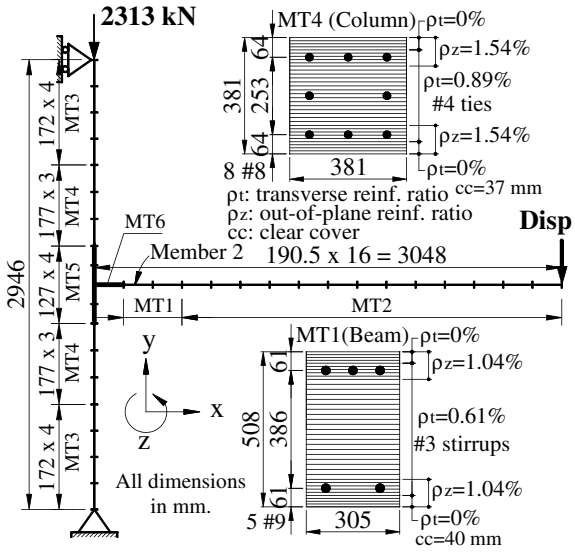

Fig. 6. Frame model and sectional models for specimens SP6 and SP7

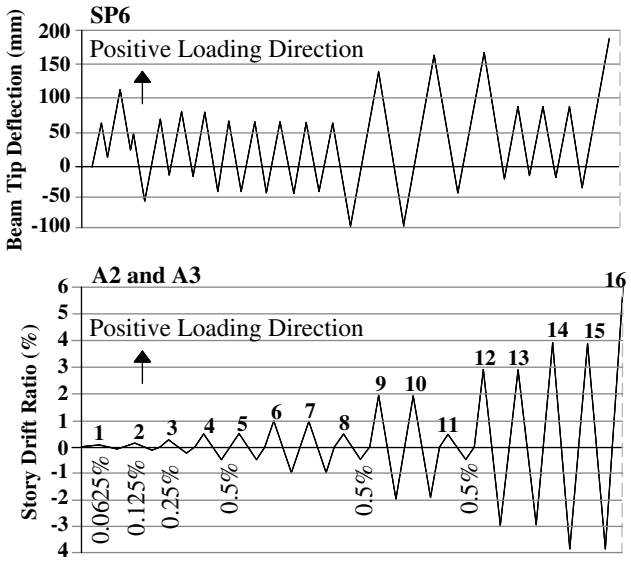

Fig. 7. Loading program applied to specimens SP6, A2, and A3

optimal accuracy. The frame models were created based on this recommendation, as shown in Fig. 6. Stiffened end zones were used to account for the overlapping portions of the beams and columns in the joint regions, as shown with bold lines in Fig. 6. For this purpose, both the longitudinal and transverse reinforcement amounts in the members within the end zones were doubled, as suggested by Guner and Vecchio (2010b). Four member types were used for the sectional models: two for the beam members with 38 concrete layers, and two for the column members with 34 concrete layers. Two additional member types were used for the stiffened end zone members, as documented by Guner (2008).

As seen in Fig. 8(a), the overall behavior of Specimen SP6 was calculated reasonably well. There is a strength degradation in the analytical response at the deflection of 126 mm. This degradation was caused by excessive flexural crack widths because the compressive strength of concrete is adversely affected by transverse cracking. The pinching characteristics of the experimental response were captured reasonably well with some underestimation. The overall behavior of Specimen SP7, shown in Fig. 8(b), was

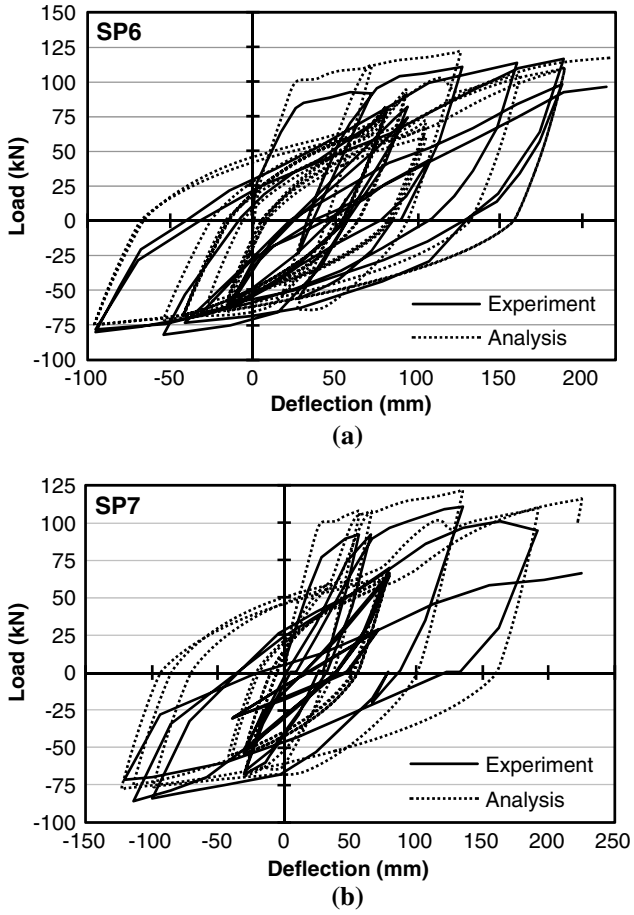

Fig. 8. Comparison of load-deflection responses for specimens: (a) SP6; (b) SP7

calculated less accurately, particularly with respect to the hysteretic pinching behavior. The reasons for this relate to the joint damage and, more importantly, to the bond slip of the top longitudinal beam reinforcement, as reported by Seckin (1981). In the analytical model, perfect bond is assumed, resulting in a stiffer and less pinched response. The slight overestimation in the initial stiffness was attributed to the irregularities in the test setup, such as imperfect support conditions and the interference of the flexibility of the loading machine. A more detailed comparison of several parameters is listed in Table 1.

The primary damage mode of Specimen SP6, observed in the experiment, involved flexural plastic hinging in the beam section close to the joint core region. A similar damage mode involving Member 2 was found analytically with crack widths as large as 10 mm and tensile reinforcement strains reaching 35.5×10^{-3}. Similar to Specimen SP6, a damage mode involving flexural plastic hinging of the beam close to the beam-column joint core was calculated for Specimen SP7, consistent with that observed in the experiment.

The second set of specimens examined was those tested by Shiohara and Kusuhara (2006), involving a number of interior beam-column subassemblies. Examined here are Specimens A2 and A3, both of which sustained the least joint core distress among all specimens in this experimental program. Both specimens had identical details, except in the load application points, as shown in Fig. 9. The test protocol involved the application of a horizontal load in a displacement-controlled mode, with the loading history shown in Fig. 7, and a constant axial force at the top of the columns.

The frame model for these specimens was created with member lengths in the range of one-half of the cross-section depths, as shown in Fig. 9. Four member types were used to create the sectional models with 31 concrete layers each. Complete details of the models can be found in Guner (2008).

As shown in Fig. 10, the overall behaviors of the subassemblies were simulated reasonably well. The strength degradation under repeated cycles at the same displacement amplitude was computed accurately for Specimen A3. There is a reduction in the load capacity in the second cycle at each displacement amplitude in Fig. 10(b). This degradation, also observed in the experiment, was primarily caused by the excessive shear straining that occurred in Member 9. Similar degradation was calculated for Specimen A2, as seen in Fig. 10(a), which somewhat overestimated the experimental degradation. As presented in Table 1, the strengths of Specimens A2 and A3 were calculated with excellent accuracy in both loading directions. The general tendency in the analytical responses was to slightly underestimate deflections at the initial stages of the loading. The analyses of these subassemblies with a more rigorous finite-element tool also provided similarly stiff responses (Sagbas et al. 2011). The total energies dissipated by the specimens were calculated with a slight overestimation, which was caused by the underestimation of the pinching in the load-deflection responses. The reason for this relates to the considerable joint core damage incurred by the specimens, as reported by Shiohara and Kusuhara (2006), which was neglected in the analysis.

The damage mode of Specimen A2 was accurately found to be flexure-shear in nature. Significant flexural damage was calculated for Member 10, with the tensile beam reinforcement strains reaching 45×10^{-3} with 6 mm concrete crack widths. More importantly, Member 9 suffered intensive diagonal shear cracking with widths up to 9 mm. An attempt to perform a third cycle of 58.8 mm displacement caused the failure of Member 9 in shear. Similarly, a flexure-shear damage mode was found for Specimen A3, consistent with experimental observation.

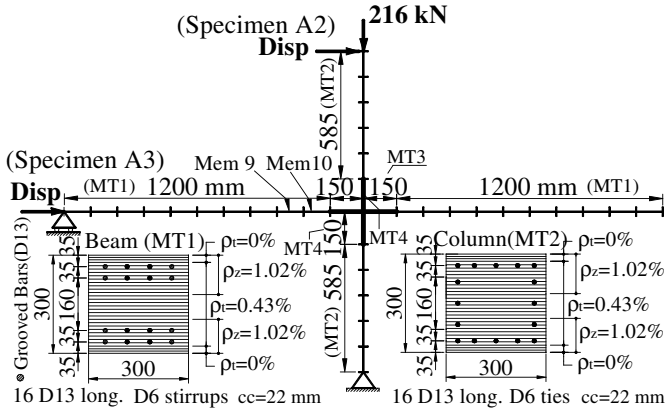

Fig. 9. Frame model and sectional models for specimens A2 and A3

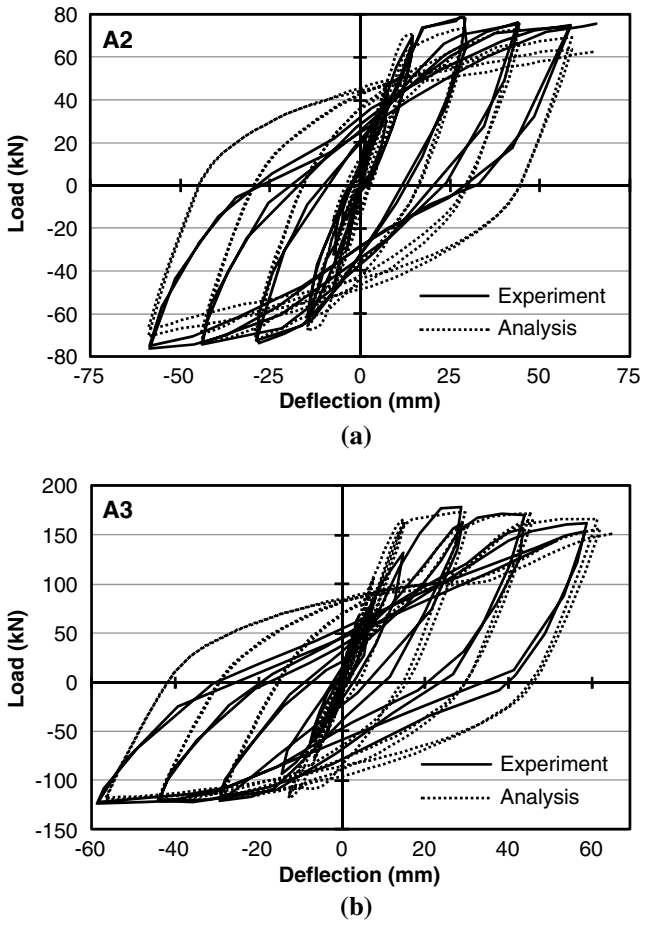

Fig. 10. Comparison of load-deflection responses for specimens: (a) A2; (b) A3

Application to Shear Walls

A set of shear wall specimens tested by Oesterle et al. (1976) was studied. The tests involved several barbell-, flange-, and rectangular-shaped shear walls, representing 1/3-scale models of five story shear walls, as shown in Fig. 11(a). Six specimens were selected for analysis, with the selection made on the basis of the availability of the experimental results. Some shear walls were omitted because of the deficiencies in the experiment, such as out-of-plane deflections, as reported by Oesterle et al. (1976). The walls were subjected to lateral loads applied to the top beams in a displacement-controlled mode to create reversed-cyclic loading conditions with displacement amplitude increments of 25.4 mm. In Walls B7 and B8, a constant vertical axial load of 1,200 kN was applied to the top loading beams.

Frame models of the walls were created with members of varying lengths, as shown in Fig. 11(b). A member length of 175 mm was used toward the base of the walls where a concentration of

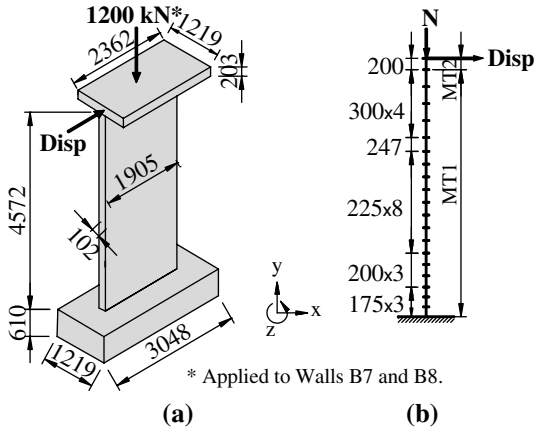

Fig. 11. PCA walls: (a) typical view (with rectangular cross section); (b) frame model

plastic deformation was expected. For shear wall structures, Guner (2008) recommended that member lengths in the range of 10% of the cross-section height be used. (This recommendation is based on a limited parametric study including only flexure-critical shear walls; shear-critical shear walls should also be investigated to reach a more general recommendation.) The member lengths were gradually increased toward the top of the walls. The base blocks of the walls were not modeled; rather, the walls were assumed to be fixed at the bases. One member type (MT1), with approximately 90 concrete layers, was used for the sectional models, as presented in Fig. 12.

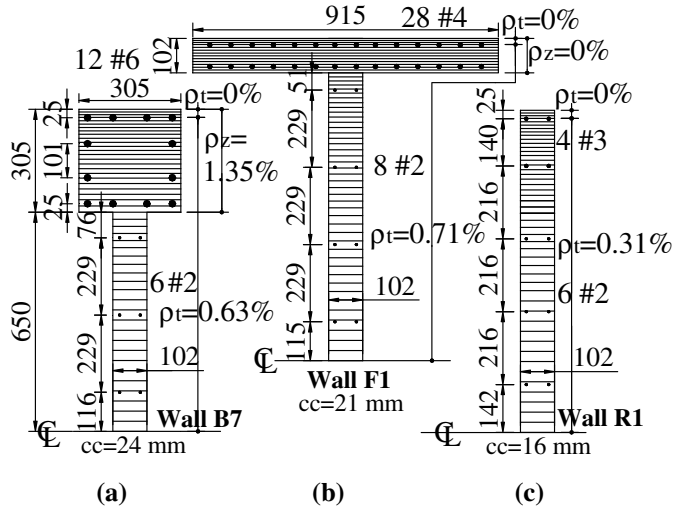

Fig. 12. Sectional models for PCA walls: (a) barbell; (b) flange; (c) rectangular

All walls exhibited flexure-dominated behaviors in both the analyses and the experiments, clear from the flat-top load-deflection curves shown in Fig. 13, except for Wall F1, which suffered a sudden shear-induced web-crushing failure before reaching its flexural strength. Generally, the overall load-deflection responses of the walls were calculated with reasonable accuracy. The pinched behavior in the experimental responses was underestimated in the analyses for Walls B1, B2, R1, and F1, but estimated more accurately for Walls B7 and B8. The latter two were the only walls tested under a constant axial force. Because of the compression, less cracking in the base and less, if any, rebar strain penetration is expected for those walls. Therefore, the analytical assumption of a perfectly fixed base and of perfect bond becomes more realistic.

The strengths of the walls were calculated reasonably accurately, as tabulated in Table 1. The slight underestimation of strength can be attributed to the stockiness of the walls, which, with a height-to-width ratio of 2.4, are at the transition point where direct strut action begins to play a more dominant role than the beam action assumed in the sectional analyses. Also evident from Table 1 is that the total energy dissipated by the walls was estimated with reasonable accuracy. The experimentally observed damage mode of Walls B1 and B2 included significant longitudinal reinforcement yielding, concrete web crushing, and reinforcement buckling. The analysis results similarly indicated significant reinforcement straining in the lowermost member, with as much as 51.5×10^{-3} strains and 9.2 mm concrete flexural crack widths. Some concrete crushing at the compression toe was calculated but to a lesser extent than experimentally observed. In the experiments, web crushing and reinforcement buckling occurred almost simultaneously, contributing to one another. However, reinforcement buckling is not taken into account by the analysis procedure employed. The damage modes of the Walls B7 and B8 were reported to include flexural mechanisms with significant web crushing. Similar

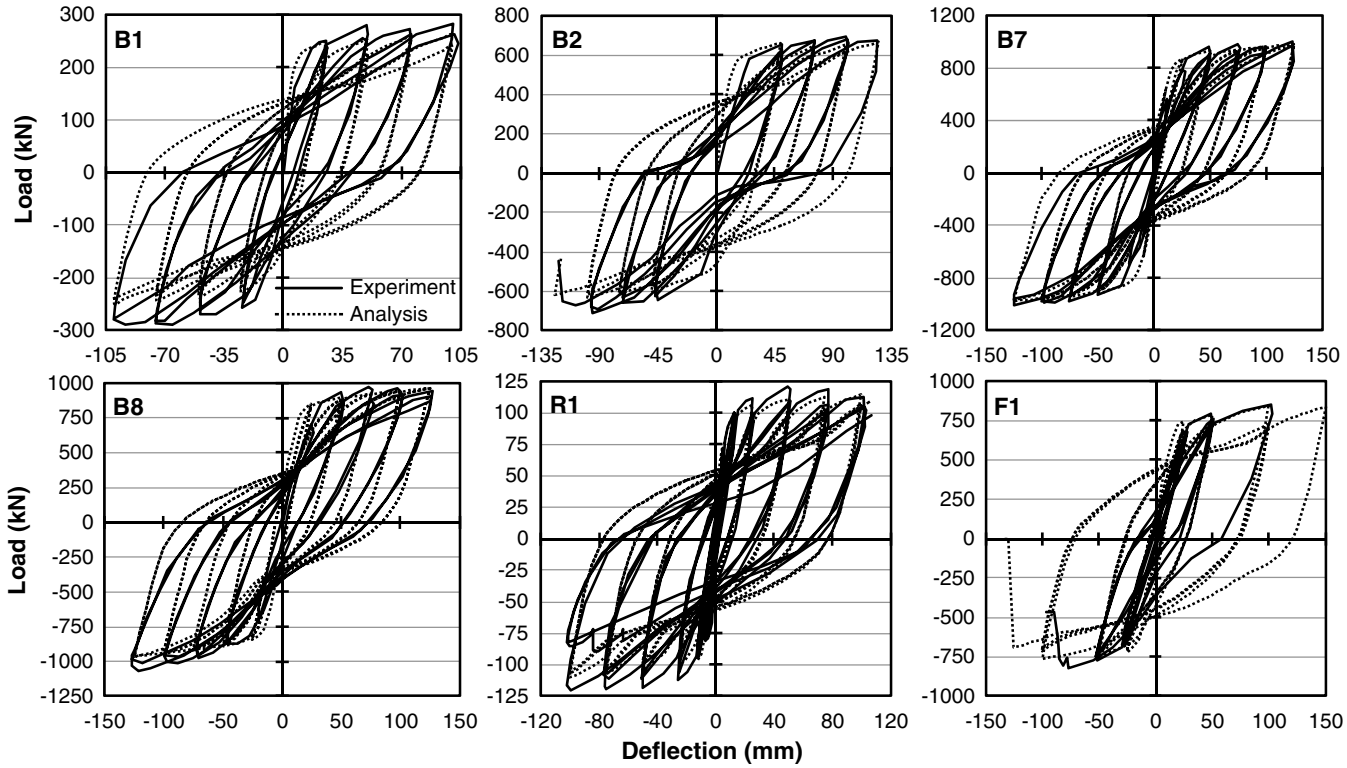

Fig. 13. Comparison of load-deflection responses for PCA walls

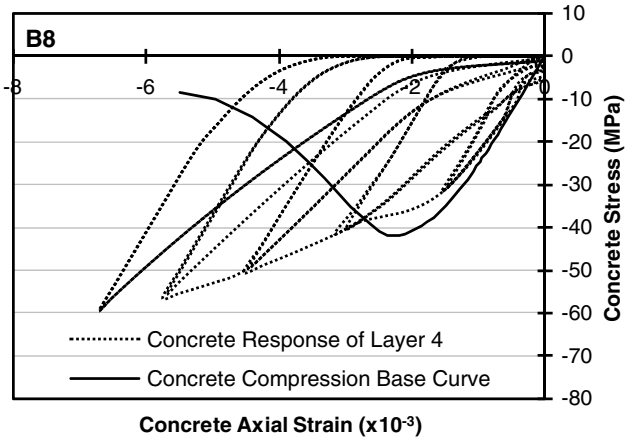

Fig. 14. Compressive response of concrete Layer 4

results were obtained analytically, but the crushing of the web concrete was calculated for Wall B8 at a larger displacement level than was in the experiment.

The experimental failure mechanism of Wall R1 was initiated by two bars buckling at approximately +75 mm lateral displacement. Both buckled bars then fractured in the following negative cycle, which is also evident in the experimental response in Fig. 13 at approximately −63 mm and −83 mm. Such a mechanism is not accounted for in the analytical procedure. As a result, the damage mode is calculated to involve the plastic hinging with significant cracking and longitudinal straining as much as 55.0×10^{-3} at a lateral displacement of 100 mm. The experimentally observed failure mechanism of Wall F1 included a sudden crushing of the web concrete at approximately −90 mm displacement, clear from Fig. 13. The analysis results indicated similar web crushing occurring at about −125 mm, as shown in Fig. 13.

Of particular interest in the behavior of these walls is the influence of the out-of-plane confinement effects in the concrete. As documented by Guner and Vecchio (2010a), out-of-plane reinforcement stresses are considered in the sectional analyses to simulate the confinement effects. Consider the response of concrete Layer 4 of Wall B8, as shown in Fig. 14; this layer was well confined with 1.35% out-of-plane reinforcement ratio. As compared to the base curve, a strength enhancement of 43% was realized for this layer in the analysis. More importantly, the strain corresponding to the peak stress was enhanced by a factor of 2.8. It is significant that such influential 3D stress effects were successfully taken into account within a 2D analysis procedure.

Current Limitations and Recommendations for Future Work

As is common in frame analyses of this type, the procedure developed uses centerline dimensions of cross sections together with stiffened joint core members. Therefore, failure modes involving beam-column joint cores cannot be captured. Such failures are typically associated with joints having improper reinforcement detailing or insufficient confinement. A nonlinear member type specifically developed for beam-column joints is required to further improve the capabilities of the proposed procedure; future work will be directed in this area. For the present, however, it is advisable to inspect the reinforcement detailing inside the joint core. In the case of unusual or improper detailing, or in cases in which analysis results indicate possible joint distress, a detailed nonlinear finite-element analysis of the joint should be undertaken. In such analyses, sectional forces obtained from the proposed procedure can be used because they will provide more realistic estimates of the boundary forces than would otherwise be obtained from linear-elastic analyses. A detailed discussion of the application of finite-element procedures for frame joints can be found in Sagbas et al. (2011).

The proposed procedure assumes perfect bond between the concrete and reinforcement; therefore, bond slip of reinforcing bars is neglected. Bond slip mechanisms are known to be particularly significant for beam-column joint cores under cyclic loads. In this study, this omission typically resulted in underestimations of the experimental pinching behaviors. In addition, provisions for longitudinal reinforcement buckling are not currently incorporated. Reinforcement buckling tends to be significant for flexure-critical columns and shear walls in the advanced stages of cyclic loading. In this study, this omission resulted in slight underestimation of cyclic damage occurred in some of the shear wall specimens. Future work will undertake to include both mechanisms into the procedure proposed.

Discussion of Results

Considering all 11 structures examined, in a displacement-controlled mode, in both the positive and negative loading directions, comprising 22 simulations, a mean of 0.96 and a coefficient of variation (COV) of 5.9% were achieved for the calculated-to-observed strength ratios. For the displacements corresponding to the peak load capacities, a mean of 1.07 and a COV of 23.7% were realized. Most of the load-deflection responses had near flat-top responses, thus making them susceptible to large errors in estimating the displacements at the peak loads. For the total energy dissipation, a mean of 1.16 with a COV of 10.6% was attained. These ratios can be regarded as satisfactory, particularly because several of the structures considered were influenced by complex second-order mechanisms; the two-story frame and the beam-column subassemblies, in particular, were heavily influenced by shear-related mechanisms. The failure modes of the structures were calculated accurately for the majority of the specimens. A failure mode that was contradictory to the experimental observations (e.g., shear failure rather than flexural failure or vice versa) was never obtained. Computed parameters, such as reinforcement strain responses, member elongations, and crack widths, showed strong correlations with the experimental results.

All analyses were performed by using the default material behavior models and analysis options, as detailed in Guner (2008); no decisions regarding the anticipated failure mode or preanalysis supporting calculations, such as sectional response hysteresis, were made. In addition, all analyses concluded without any numerical stability problems and in a short period of time. The complete analysis of a PCA shear wall, for example, required a computation time of approximately 20 min [on a laptop computer with an Intel Dual Core 2 Duo T7500 (2.2 GHz) processor, 2 GB DDR2 (677 MHz) RAM, and a 7,200 RPM hard disk drive]. This is significant considering the several hours required for such analyses using 2D finite-element procedures. Moreover, the relatively irregular loading protocol of Specimen SP6 was successfully simulated through the use of seed files (i.e., binary input files). Finally, the previously implemented shear protection algorithm (Guner and Vecchio 2010a), which prevents premature failures of D-regions, performed well under cyclic loads.

Summary and Conclusions

A nonlinear frame analysis procedure previously developed for monotonic loading is further developed to consider general loading conditions, including the special cases of cyclic and reversed-cyclic loading. The procedure uses classical stiffness-based linear-elastic frame analysis algorithms in a nonlinear mode based on an unbalanced force approach. A total-load secant-stiffness analysis algorithm is employed, as opposed to the more commonly used incremental-load tangent-stiffness approach. Rigorous nonlinear sectional analyses of concrete member cross sections, using a layered element approach, are undertaken on the basis of the realistic hysteresis models implemented for the concrete and reinforcement. An incremental formulation is used to track concrete stress and strain histories. Transverse shear effects are included through a 2D implementation of the disturbed stress field model, which is based on a smeared rotating crack conceptualization. As such, it complements other available methodologies, such as Petrangeli's formulation based on a microplane model. Advantages of the proposed procedure were demonstrated. Among them are the intrinsic and accurate consideration of shear effects and other important second-order mechanisms and the simple modeling requirements that make it suitable for use by practicing structural engineers. The proposed analytical model was verified with a variety of previously tested specimens, including one large-scale frame, four large-scale beam-column subassemblies, and six 1/3-scale shear walls. The results of the studies conducted support the following conclusions:

1. The omission of shear-related mechanisms in reinforced concrete frame analyses can lead to grossly inaccurate and unsafe predictions of strength and ductility when evaluating structural performance under cyclic loading.
2. Classical stiffness-based frame analysis algorithms continue to provide a simple, fast, and accurate analytical base for the implementation of nonlinear fiber models.
3. A total-load secant-stiffness formulation provides a reliable platform for simulations of nonlinear frame behavior under general loading, when implemented into a nonlinear frame analysis algorithm.
4. The constitutive models previously developed for general load analysis of concrete continuum structures, based on a smeared rotating crack conceptualization, produce accurate simulations of nonlinear frame behavior under general loading, when implemented into a layered-element sectional analysis algorithm.
5. Consideration of significant second-order mechanisms, such as out-of-plane confinement effects and reinforcement dowel action, is necessary for accurate simulations of frame response.
6. The analytical procedure developed accurately simulates the overall experimental responses of frame structures subjected to cyclic and reversed-cyclic loading. Strengths, stiffnesses, ductilities, and failure modes are captured accurately. Computed parameters, such as crack widths, reinforcement strains, and member deformations, are also simulated well.
7. The analytical procedure developed exhibits excellent convergence and numerical stability characteristics, requiring little computational time for analyses under general loading.
8. Further work is required to accurately model the behavior of frames heavily influenced by joint core distress, reinforcement bond slip, or compression bar buckling. In addition, more analytical verification studies should be undertaken to further investigate the optimum segment length recommendations, in particular, for shear wall structures.

References

Bairan, J. M., and Mari, A. R. (2007). "Multiaxial-coupled analysis of RC cross-sections subjected to combined forces." *Eng. Struct.*, 29(8), 1722–1738.

Bazant, Z. P., and Bhat, P. D. (1977). "Prediction of hysteresis of reinforced concrete members." *J. Struct. Div.*, 103(1), 153–167.

Bentz, E. C. (2000). "Sectional analysis of reinforced concrete members." Ph.D. thesis, Dept. of Civil Engineering, Univ. of Toronto, 310.

Ceresa, P., Petrini, L., Pinho, R., and Sousa, R. (2009). "A fibre flexure–shear model for seismic analysis of RC-framed structures." *Earthquake Eng. Struct. Dyn.*, 38(5), 565–586.

Duong, K. V., Sheikh, S. A., and Vecchio, F. J. (2007). "Seismic behavior of shear-critical reinforced concrete frame: Experimental investigation." *ACI Struct. J.*, 104(3), 304–313.

European Committee for Standardization (CEN). (1991). "Design of concrete structures—Part 1.1: General rules and rules for buildings." *Eurocode 2*, *ENV 1992-1-1*, Brussels, Belgium.

Filippou, F. C., and Saritas, A. (2006). "A beam finite element for shear-critical RC beams." *SP-237-19*, American Concrete Institute, Detroit, 295–309.

Guner, S. (2008). "Performance assessment of shear-critical reinforced concrete plane frames." Ph.D. thesis, Dept. of Civil Engineering, Univ. of Toronto, ⟨http://www.civ.utoronto.ca/vector⟩ (Jun. 20, 2011), 429.

Guner, S., and Vecchio, F. J. (2008). "User's manual of VecTor5." ⟨http://www.civ.utoronto.ca/vector/⟩ (Jun. 20, 2011), 88.

Guner, S., and Vecchio, F. J. (2010a). "Pushover analysis of shear-critical frames: Formulation." *ACI Struct. J.*, 107(1), 63–71.

Guner, S., and Vecchio, F. J. (2010b). "Pushover analysis of shear-critical frames: Verification and application." *ACI Struct. J.*, 107(1), 72–81.

Marini, A., and Spacone, E. (2006). "Analysis of reinforced concrete elements including shear effects." *ACI Struct. J.*, 103(5), 645–655.

Mostafaei, H., and Vecchio, F. J. (2008). "Uniaxial shear-flexure model for reinforced concrete elements." *J. Struct. Eng.*, 134(9), 1538–1547.

Oesterle, R. G., Fiorato, A. E., Johal, L. S., Carpenter, J. E., Russell, H. G., and Corley, W. G. (1976). "Earthquake resistant structural walls—Tests of isolated walls." Construction Technology Laboratories, Portland Cement Association, Skokie, IL, 315.

Palermo, D., and Vecchio, F. J. (2003). "Compression field modeling of reinforced concrete subjected to reversed loading: Formulation." *ACI Struct. J.*, 100(5), 616–625.

Petrangeli, M., Pinto, P. E., and Ciampi, V. (1999). "Fiber element for cyclic bending and shear of RC structures. I: Theory." *J. Eng. Mech.*, 125(9), 994–1001.

Rericha, P. (1991). "Layer model of bending-shear failure in RC plates and beams." *J. Struct. Eng.*, 117(10), 2865–2883.

Sagbas, G., Vecchio, F. J., and Christopoulos, C. (2011). "Computational modeling of the seismic performance of beam-column subassemblies." *J. Earthquake Eng.*, 15(4), 640–663.

Seckin, M. (1981). "Hysteretic behavior of cast-in-place exterior beam-column-slab subassemblies." Ph.D. thesis, Dept. of Civil Engineering, Univ. of Toronto, 236.

Shiohara, H., and Kusuhara, F. (2006). "Benchmark Test for Validation of Mathematical Models for Non-linear and Cyclic Behavior of R/C Beam-column Joints." ⟨http://www.rcs.arch.t.u-tokyo.ac.jp/shiohara/benchmark/test_report.pdf⟩ (Jun. 20, 2011), 126.

Vecchio, F. J. (1999). "Towards cyclic load modeling of reinforced concrete." *ACI Struct. J.*, 96(2), 193–202.

Vecchio, F. J. (2000). "Disturbed stress field model for reinforced concrete: Formulation." *J. Struct. Eng.*, 126(9), 1070–1077.

Vecchio, F. J., and Collins, M. P. (1988). "Predicting the response of reinforced concrete beams subjected to shear using modified compression field theory." *ACI Struct. J.*, 85(3), 258–268.